JOURNAL OF SPACECRAFT AND ROCKETS
Vol. 31, No. 5, September–October 1994

Uranus and Neptune Atmospheric-Entry Probe Study

M. Tauber,* P. Wercinski,† W. Henline,‡ and J. Paterson§
NASA Ames Research Center, Moffett Field, California 94035
and
L. Yang¶
Sterling Software, Palo Alto, California 94303

Entry trajectories, decelerations, and heating and heat shielding requirements of probes entering the atmospheres of Uranus and Neptune at velocities up to 26.5 km/s were studied. Much of the Galileo Jupiter probe technology was applicable to these outer-planet probes; therefore, the same configuration was used. Steep (ballistic) entry flight-path angles were needed to facilitate communication from the probes to the spacecraft during atmospheric descent. The Galileo probe's 400 *g* maximum deceleration structural design was used to define the maximum entry angles for the Uranus and Neptune probes. The carbon phenolic heat shield material used on the Galileo and the successful Pioneer-Venus probes was selected. Turbulent boundary-layer convection dominated the heating of the Uranus and Neptune probes; radiative heating was negligible by comparison. The peak heating rates were found to be about 6 kW/cm^2, or approximately 25% of the Galileo probe's expected maximum value. The forebody heat shield mass fractions for these outer-planet probes were found to vary from about 0.08 to 0.16 for entry velocities from 22 to 26.5 km/s. By comparison, the Pioneer-Venus probes' heat shield mass fractions ranged from 0.10 to 0.13, and the Galileo probe's forebody value is 0.43.

Nomenclature

A	= reference (cross-sectional) area of entry vehicle, m^2
C_D	= drag coefficient, based on area A
m/C_DA	= ballistic coefficient of vehicle at entry, kg/m^2
m_E	= mass of vehicle at entry, kg
m_{HS}	= mass of forebody heat shield at entry, kg
$(\text{mol. wt.})_w$	= molecular weight of atmospheric gas at wall conditions
Pr_w	= Prandtl number of atmospheric gas at wall conditions
$\dot{q}_l$	= laminar heat transfer rate, W/cm^2
$\dot{q}_t$	= turbulent heat transfer rate, W/cm^2
R_b	= base radius, m
Re_{bt}	= boundary-layer edge Reynolds number at beginning of transition
R_n	= nose radius, m
S	= distance along surface from stagnation point, m
V_e	= entry velocity relative to rotating atmosphere, km/s
V_{Ei}	= entry velocity in inertial reference frame, km/s
V_{Er}	= entry velocity relative to rotating atmosphere, km/s
V_{ESC}	= escape velocity from planet at given altitude, km/s
V_{HE}	= hyperbolic excess velocity of vehicle, km/s
γ_{Er}	= entry flight-path angle at given altitude and relative to rotating atmosphere, deg
μ_w	= coefficient of viscosity of atmospheric gas at wall conditions, kg/m · s

Presented as Paper 93-3689 at the AIAA Atmospheric Flight Mechanics Conference, Monterey, CA, Aug. 9–11, 1993; received Aug. 17, 1993; revision received Jan. 3, 1994; accepted for publication Jan. 5, 1994.

*Research Scientist. Associate Fellow AIAA.
†Research Scientist. Member AIAA.
‡Research Scientist. Senior Member AIAA.
§Ames Associate.
¶Research Specialist. Member AIAA.

Introduction

THE Voyager spacecraft flew past the gaseous outer planets Uranus and Neptune in January 1986 and August 1989, respectively. The vast amount of new scientific data obtained during the flybys of both planetary systems has stimulated much interest in further exploration, especially of the planets' active atmospheres.[1] Toward this end, NASA Headquarters funded studies of atmospheric entry probes to both planets.[2,3] The objectives of the probe missions are to perform in situ measurements of the planets' atmospheres to pressure levels of 75 to 100 bars. These pressures occur at altitudes that are well below the methane, ammonia, hydrogen sulfide, and water clouds that are believed to exist. However, the probes must be aerodynamically decelerated prior to making atmospheric measurements.

The anticipated atmospheric entry velocities at Uranus and Neptune will be roughly one-half the 48 km/s speed of the Galileo probe relative to Jupiter's rotating atmosphere. The atmospheric compositions of all three planets are very similar. Jupiter's atmosphere is 89% hydrogen and 11% helium, Uranus's is 85% and 15%, and Neptune's is 81% and 19%. In the interest of economy, it has been proposed[2,3] that maximum use be made of the Galileo probe technology base and that the same basic configuration be used for the Uranus and Neptune entry vehicles. However, the lower entry velocities of the outer-planet probes should result in substantially lighter heat shields than Galileo's. The entry probe studies presented in Refs. 2 and 3 contained estimates of heat shielding requirements for Uranus and Neptune probes that used information that was published in 1971.[4] These calculations[4] were based on the very limited knowledge of the outer planets' atmospheric properties that were available around 1970. The more recent Voyager flyby measurements of Uranus's and Neptune's atmospheric structures and compositions have enabled making more precise calculations of the atmospheric deceleration environments. The objectives of the present study are to use the current atmospheric data to compute parametrically the Uranus and Neptune entry trajectories, deceleration pulses, forebody heating rates, and total heat loads. The results of the heating calculations will be used to estimate the forebody heat shield mass ratios. The same carbon phenolic heat shielding material that was used on the Galileo probe and on the four successful Pioneer-Venus probes will be utilized in the study.

Atmospheric Trajectories

The outer-planet probes in this study were targeted and deployed from a carrier spacecraft "bus" while on hyperbolic approach tra-

jectories, well in advance the spacecraft's planetary encounter. Targeting was partially constrained by the need to avoid planetary rings by the probe and the bus. Previously, missions have been studied[3] where the bus flew past the planet, or where the bus was propulsively decelerated into planetary orbit. In both scenarios, communication from the probe to the bus during atmospheric descent occurred prior to insertion into orbit. A time of about 1.5 hr was required for the probes to descend to the 75- to 100-bar pressure levels.[3] During descent, the probe was entrained by the rotating atmosphere. To insure line-of-sight relay communications with the bus during the atmospheric measurement phase of the mission, a steep entry flight-path angle was needed. To take advantage of the Galileo capsule's aeroshell structural design heritage, the peak deceleration had to be limited to 405 Earth g. For a given entry velocity relative to the rotating atmosphere, the flight-path angles at entry were constrained in the study to obey a design deceleration limit of 400 g. However, it was recognized that the structural design also depended on the probe's mass and on the peak pressure value and its distribution on the face of the aeroshell. Although the present nominal probe's mass of 290 kg differed from the Galileo probe's entry mass of 339 kg, by the time that the Galileo probe reaches peak deceleration, extensive ablation will have reduced Galileo's mass to about the same value as that of the nominal Uranus and Neptune probes. (Peak heating always occurs prior to the point in the trajectory where maximum deceleration and peak pressure are encountered.) Therefore, the deceleration forces on the probe's structures may be very similar at these three outer planets.

The entry vehicle configuration is similar to that of the Galileo probe, which was a spherically blunted 45 deg half-angle cone (see Fig. 1). The major difference was the thinner carbon phenolic heat shield. The base diameter of 1.25 m was held constant for all probes, as was the hypervelocity drag coefficient value of 1.05. However, below Mach 3 the drag coefficient was varied with the Mach number. A nominal ballistic coefficient at entry of 225 kg/m^2 was used; the corresponding entry mass was 289.9 kg. For the minimum and maximum ballistic coefficients of 150 and 300 kg/m^2, the probes' masses at entry were 193.3 and 386.6 kg, respectively.

As a probe approaches the planet along a hyperbolic trajectory, the planet's massive gravitational field accelerates the entry capsule. The inertial atmospheric entry velocity is a function of the interplanetary trajectory and the planet's gravitational potential. The assumed arrival conditions are for a range of interplanetary trajectories[3,5] with arrival dates at Uranus and Neptune occurring between 2013 and 2021. The interplanetary trajectories assume a Titan IV–Centaur launch vehicle and employ multiple swingby accelerations at Earth, Venus, and Jupiter. The ranges of inertial entry velocities V_{Ei} at a specified altitude (500 km at Uranus and 450 km at Neptune, measured relative to the 1-bar pressure levels) are approximately 25 to 26 km/s at Uranus and 24 to 27 km/s at Neptune.

The trajectory of the probe is dependent on the entry velocity and flight-path angle relative to the planet's rotating atmosphere and on the atmospheric structure. The relative flight conditions are a complex function of the planet's rotation rate and the latitude, altitude,

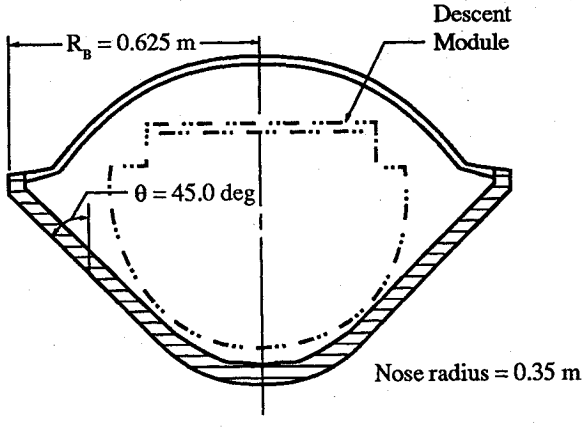

Fig. 1 Neptune and Uranus probe configuration (heat shield thickness not to scale).

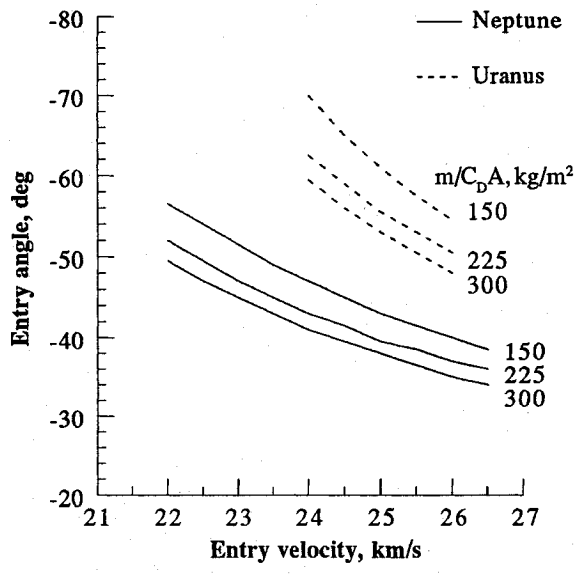

Fig. 2 Entry angle as a function of entry velocity for ballistic entry with 400-g peak declaration limit.

and azimuthal direction at entry, in addition to the probe's velocity and flight-path angle in the inertial reference frame. The planetary atmospheric structures used were based on Voyager data,[3,5] and the entry latitude and azimuthal direction used were from Ref. 3. For the mission time frames studied, the ranges of relative entry velocities V_{Er} were found to be 24 to 26 km/s at Uranus and 22 to 26.5 km/s at Neptune. To reduce the number of variables in the analysis, the steepest flight-path angle for a particular relative entry angle was calculated. The flight-path angles obeyed the 400-g limit and are shown in Fig. 2 for ballistic coefficients (m/C_DA) from 150 to 300 kg/m^2. The probe was assumed to fly at zero angle of attack. The relative flight conditions were used to compute the atmospheric forces and heating on the entry probes.

Examples of entry trajectories were calculated for nominal missions[3] (velocities near the upper end of the speed range were chosen to be conservative) at Uranus and Neptune and are shown in Figs. 3a and 3b. As can be seen from Fig. 3 and even more clearly from Fig. 4, the atmospheric deceleration periods are only about 15 s in duration, since the flight-path angles were steep. In the computation of the trajectories, the probes' mass losses from heat shield ablation, and the resulting decrease in ballistic coefficient, were taken into account. Because the mass losses were modest (as will be discussed later), the influence of ablation on the trajectories was small. When the probe decelerated to subsonic speed, a parachute was deployed that pulled the instrumented descent module from the hot aeroshell, which was discarded. To take full advantage of Galileo technology, the same parachute design was stipulated in the present study. The Galileo parachute was qualified for deployment at a dynamic pressure of 0.06 atm, with a factor of safety of 1.5. For the nominal trajectories shown in Fig. 3, the parachute deployment and aeroshell separation procedure was assumed to occur near the maximum design pressure at subsonic speeds about 1–2 min after entry.

Shock Layer Parameters

The approximately 26 km/s relative entry velocities at Uranus and Neptune were more than twice as large as the entry velocities experienced by the Apollo capsules returning from the moon (11 km/s) or the Pioneer-Venus probes upon entering that planet's atmosphere (11.5 km/s). However, the hydrogen-rich atmospheres of the outer planets have much higher specific heats than air or the Venusian carbon dioxide atmosphere, since the specific heats are inversely proportional to the molecular weights of the gases. In addition, the dissociation energy of hydrogen is significantly lower than that of nitrogen, oxygen, or carbon dioxide. Therefore, the temperatures within the shock layer of an outer-planet probe will be much lower than in air, or the Venusian atmosphere, at the same flight speed. Since the shock layer gas temperatures and densities determine the

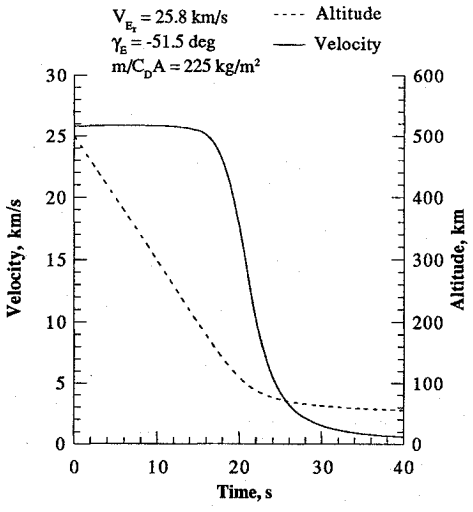

a) Uranus

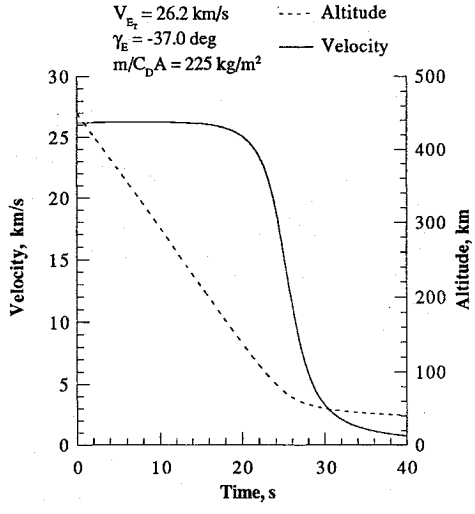

b) Neptune

Fig. 3 Trajectory parameters for nominal entry conditions.

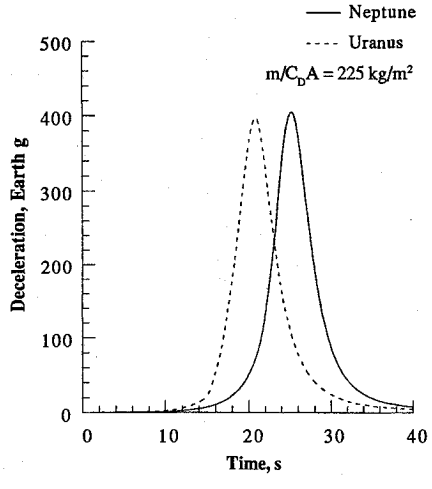

Fig. 4 Declaration profiles for nominal entry trajectories for both planets.

heating of the body, it is informative to compare these state quantities in the different gases.

The thermodynamic properties of the hydrogen-helium mixtures were computed using the code described in Ref. 6. The conditions behind the normal shock in front of a blunt body in the outer planets' atmospheres indeed were found to be much less severe than in air at the same flight conditions, as is shown in Fig. 5. Note

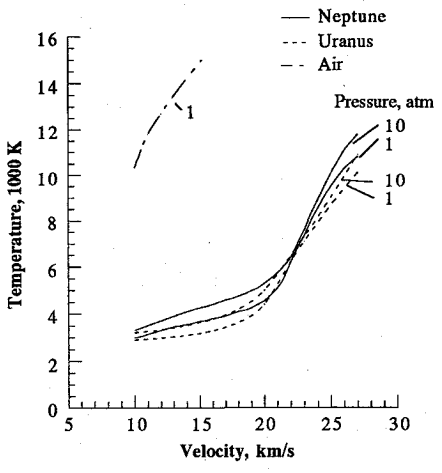

Fig. 5 Temperatures behind a normal shock for different planetary atmospheres.

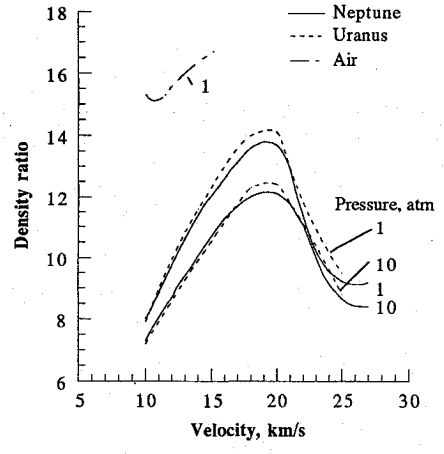

Fig. 6 Density ratios across a normal shock for different planetary atmospheres.

that the shock layer temperature at the Apollo lunar return speed of 11 km/s is 12,000 K in air, compared to about 3500 K behind the normal portion of the bow shock in the hydrogen-helium mixtures of the outer planets. In contrast, the 12,000 K temperature was only reached at flight speeds exceeding 26 km/s in the outer planets' atmospheres. The density ratios across the normal shocks are shown in Fig. 6. Again, the ratios are substantially less in the outer planets' gases than in air, resulting in a larger shock standoff distance and therefore reduced heating rates. (The effect of the density ratio on the stagnation-point heating rates will be discussed in the next section.) The state properties that are shown in Figs. 5 and 6 were calculated for pressures of 1 and 10 atm. The stagnation pressures for the nominal trajectories at both planets reach values of about 16 atm, as shown in Fig. 7. However, the large areas of the conical frustums of the probes, where most of the heat shielding mass was required, experienced peak pressures of about 8 atm. These pressures were accompanied by high Reynolds numbers, which caused boundary-layer transition that resulted in severe heating. However, the heating was still substantially less than in air at the same speeds, as discussed in the next section.

Entry Heating Environment

Bodies entering atmospheres at very high speeds experience both radiative heating from the incandescent shock layer and convective heating from friction within the boundary layer and chemical reactions near the surface. At the low temperatures (compared to air at the same speeds) existing in the probes' shock layers, the radiative heating rates were about two orders of magnitude less[7–9] than the convective heating, and they have been neglected here.

The stagnation point laminar boundary-layer convective heating rates, in the absence of mass injection, on a body in different gases

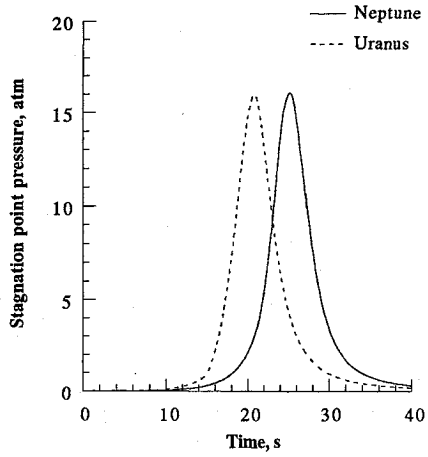

Fig. 7 Stagnation point pressure profiles for normal entry trajectories for both planets.

can be expressed[10] in terms of gas properties at the wall temperature as

$$\dot{q}_l \sim (\text{mol. wt.})_w^{0.5} \mu_w^{0.5} / Pr_w \qquad (1)$$

The molecular weights of the ambient atmospheres that were used in the present study were about 2.30 for Uranus, 2.38 for Neptune, and (for comparison) 28.9 for air. Transport properties for one hydrogen-helium mixture, representative of the Neptune atmosphere, were calculated using Ref. 11, and these values were also used for the Uranus probe. The same molecular-weight effects were responsible for the large differences in the shock-layer temperatures of probes in the outer planets' atmospheres and in air. However, the stagnation-point heating rates are inversely proportional to the fourth root of the density ratio across the bow shock.[10] The low density ratios exhibited by the hydrogen-helium mixtures, compared to air at the same speeds (see Fig. 6), increased the heating somewhat. (The variation of the stagnation-point heating rate as the fourth root of the trans-shock density ratio results from assuming a Newtonian pressure distribution when calculating the velocity gradient.[10] In addition, the stagnation-point heating rate also varies as the square root of the freestream density.)

First, the nonablative (cold-wall) stagnation point heating rates were computed by applying the hydrogen-helium gas-mixture correlation[12] to Eq. (1) that was previously derived for air.[10] The stagnation-point relations were applied on the blunt nose and the laminar-flow portion of the cone frustum by scaling the heating rate with the square root of the surface pressure and using a pressure distribution[13] based on Newtonian theory. Incipient transition to turbulence was based on the boundary-layer edge Reynolds number. A conservative nominal value of 2.5×10^5 was chosen for most cases in an attempt to allow for the destabilizing effect of mass addition and surface roughness from ablation. The effect on the heating of varying the transition Reynolds number from 10^5 to 10^6 was computed. The extent of the transitional flow region was assumed to be equal in length to the preceding laminar flow region. The heating rate within the transitional flow was assumed to vary linearly from the laminar to the fully developed turbulent value. The cold-wall turbulent boundary-layer heating was computed by starting with a flat-plate heating equation for air,[13] based on the Blasius turbulent skin friction relation, and applying a van Driest-type geometric transformation from a flat plate to a cone.[10] (The turbulent heating equation for air[13] was derived using the reference-enthalpy concept and gives conservative values.) The resulting equation was then modified for the hydrogen-helium atmospheric gas composition by using the turbulent equivalent of Eq. (1), which is

$$\dot{q}_t \sim (\text{mol. wt.})_w^{0.8} \mu_w^{0.2} / Pr_w \qquad (2)$$

The above-discussed heating relations were applicable to a nonablating wall.

Second, prior to being used, the nonablating wall heating relations were modified to take account of the presence of ablation vapor

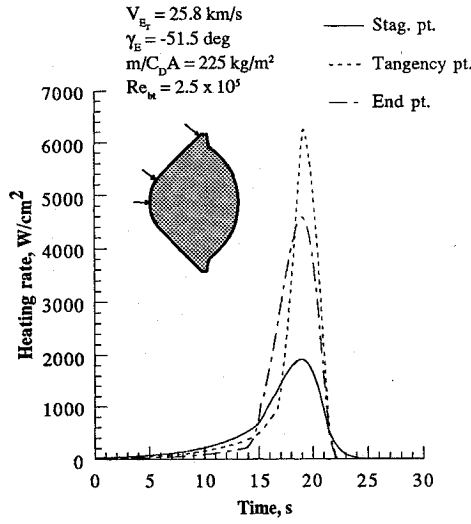

a) Uranus

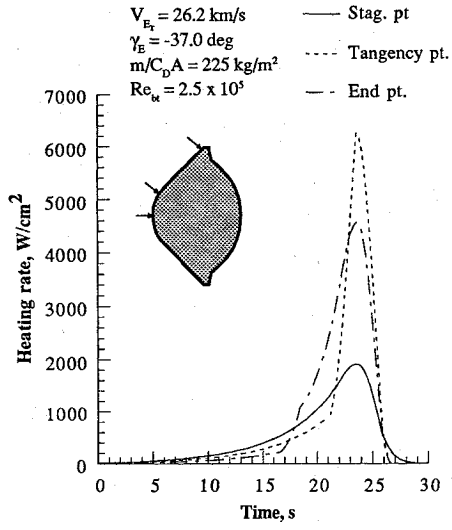

b) Neptune

Fig. 8 Heating rates at specified body locations for nominal entry trajectories.

blockage. A quadratic expression for the mass-addition (blowing) rate[14] was used to take into account the state of the boundary layer (laminar or turbulent) and the approximate molecular weights of the boundary-layer gases and the injected ablation gases. It was also assumed that the response of the carbon phenolic material could be approximately characterized by an effective heat of ablation. A value of 35 MJ/kg was used. (The use of an effective heat of ablation was justified on the basis that the peak heating rates over most of the body were sufficiently high so that the primary ablation mechanism was sublimation; char-removal mechanisms such as chemical reactions and spallation were assumed to be of secondary importance.) The approximate method described above was used to calculate the ablating surface heating rate distributions over the bodies as a function of time. Therefore, all heating rates to be discussed and shown will be for ablating surfaces.

The heat shield was assumed to be constructed of carbon phenolic as noted previously. A stagnation point nose radius of 0.35 m was used and assumed to remain constant (which is conservative), since the surface recession was found to be only a few millimeters. The ablating wall heating rates at three body points are shown in Figs. 8a and 8b for the nominal entry trajectories shown in Fig. 3 for Uranus and Neptune. Conditions at the stagnation point, the tangency point between the spherical nose cap and cone, and the end of the forebody (prior to the expansion of the flow around the corner into the wake region) are presented. Note that the severe portion of the heating pulses lasts less than 10 s and results from turbulent boundary-layer convection; the laminar stagnation-point heating rates are substan-

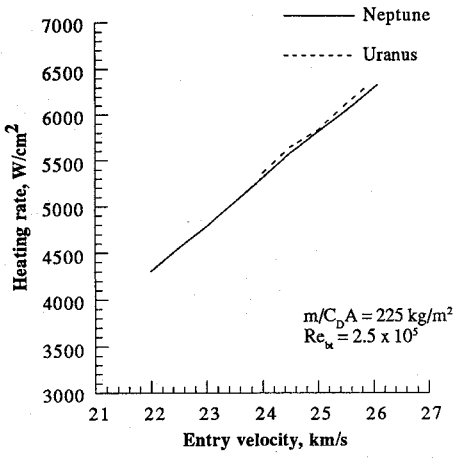

Fig. 9 Maximum heating rate values.

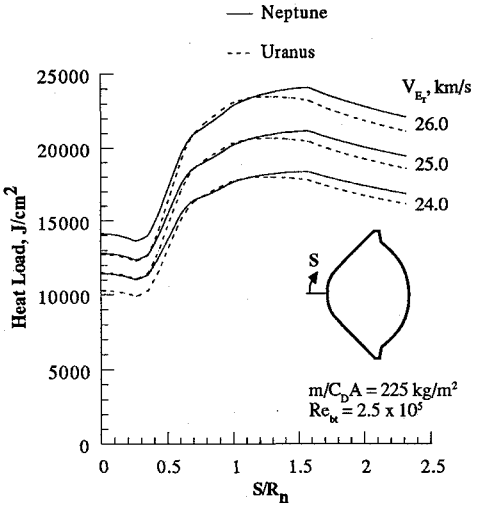

Fig. 10 Heat load distribution over the aeroshell as a function of surface location.

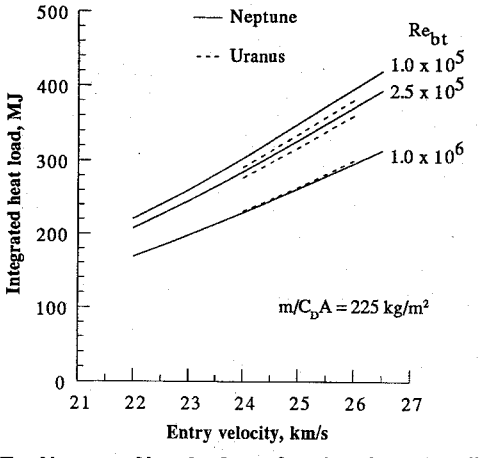

Fig. 11 Total integrated heat loads as a function of transition Reynolds number for Uranus and Neptune.

tially lower. The values shown in Fig. 8 exceed 6 kW/cm^2 at both planets, although the maximum heating rates (see Fig. 9) are slightly higher and occur on the cone frustum between the nose tangency and end points on the body.

For comparison, the stagnation point ablating-surface peak heating rate for the Galileo probe[8,15] is about 27 kW/cm^2, but consists almost exclusively of shock-layer radiation. At Jupiter, the much higher heating and the predominance of radiation are to be expected because of the much greater entry velocity.

Heat Shielding Requirements

Ablative heat shield material technology was already mature in the mid-1970s when the heat shields for the Galileo entry capsule and the Pioneer-Venus probes were designed. More recently, stronger and more shear-resistant heat shield materials, such as various forms of carbon-carbon, have been developed and tested. However, the successful Pioneer-Venus probes and the (hopefully) successful Galileo Jupiter probe entry may result in the continued use of carbon phenolic heat shielding material for outer-planet exploration. Therefore, carbon phenolic heat shielding was selected for use in the present study.

To accurately determine the mass of the heat shield, the net heating rate at a body location must be integrated over the entry time using a boundary-layer flowfield solution (BLIMPK)[16] coupled with an in-depth material response solution. By this method, the time-dependent heat conduction, pyrolysis, char removal and reradiation from the ablator can be computed. Such a labor-intensive and computationally time consuming procedure (time steps of 0.001 s were required) was impractical for the present, parametric study. Therefore, a minimum of time-dependent, numerical computations were made using the charring-material ablation (CMA) code[17] to determine heat shield thicknesses that are required to limit the temperature at the interface between the ablative material and the spacecraft structure in the Neptune entry environment. Local heat-transfer coefficients from the BLIMPK code were used as inputs to CMA along the entry trajectory. A scaling parameter was then developed from the CMA-calculated heat shield thicknesses and heat loads. The scaling parameter consisted of the heat shield mass per unit area divided by the total heat load per unit area. The scaling parameter was used in conjunction with the total heat loads that were calculated using the approximate methods described in the previous section, and was applied to both the Uranus and Neptune probes to estimate the forebody heat shielding mass fractions that were required. Therefore, the total heat loads (the ablating wall heating rates integrated over the surface and over time) had to be computed before the heat shield masses could be found.

The heating pulses shown in Fig. 8 were for relative entry velocities of about 26 km/s and a boundary-layer transition Reynolds number of 2.5×10^5. The distribution of the heat loads over the bodies is shown in Fig. 10 for relative entry velocities of 24, 25, and 26 km/s, at both planets. Note that the extensive turbulent heating on the conical frustrum causes the heat loads to be 60 to 70% higher than near the (laminar) stagnation point. The variation of total heat loads with entry velocity, transition Reynolds number, and probe ballistic coefficients is considered next. Figure 11 illustrates that the total heat load for the Neptune probe rises by about 85% as the (relative) entry velocity increases from 22 to 26.5 km/s. The rate of change of heat load is almost the same for the Uranus probe, although the entry velocity range that was considered was much smaller. Also shown in Fig. 11 is the effect of transition Reynolds number. Decreasing the transition value from 2.5×10^5 to 1.0×10^5 only raises the total heat load by 6 to 7%, while increasing the value to 1.0×10^6 results in a 20% decrease. Thus, the effect on the total heat load of varying the transition Reynolds number even by a factor of 10 is modest. In contrast, changing the nominal ballistic coefficient of 225 kg/m^2 by $\pm 33.3\%$ affects the heat load more, as is shown in Fig. 12. The heat load is close to being directly proportional to the ballistic coefficient; the exponent of the proportionality factor is about 0.9. It is also noteworthy that the heat loads were almost the same for both planets at a given entry speed, mainly because the peak decelerations were stipulated to be identical for all the trajectories.

The ablative and conductive behavior of the carbon phenolic heat shield material has been studied extensively for several decades, including its application to the Pioneer-Venus probes and the Galileo Jupiter probe.[18] In view of the high pressure forces acting on the heat shields that were considered here, it was decided not to attempt to use a low-density insulative material between the carbon phenolic and the aluminum forebody structure. Instead it was assumed that the carbon phenolic would be bonded directly to the aluminum structure, as was done for the Pioneer-Venus and Galileo probes. Therefore, a sufficient amount of virgin carbon phenolic had to remain after the cessation of the heating pulses to act as insulation and prevent

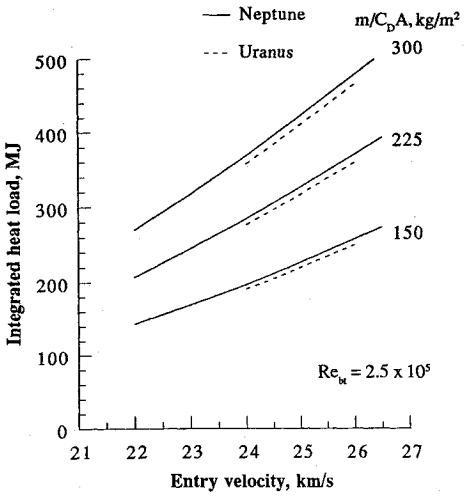

Fig. 12 Total integrated heat loads as functions of ballistic coefficient for Uranus and Neptune.

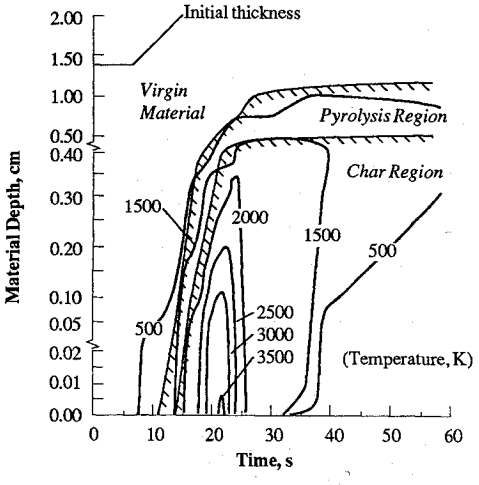

Fig. 13 In-depth temperature distribution profile (from CMA) at the stagnation point for carbon phenolic for nominal Neptune entry. (Note scale changes on ordinate.)

the temperature at the back face of the heat shield, adjacent to the aluminum structure, from exceeding 500 K. (For heating durations on the order of minutes, AL-2024-T81, for example, experiences less than 20% degradation in strength at 500 K, and commonly used adhesives such as RTV-560 function well to temperatures of 560 K.[19])

A back-face wall temperature limit of 500 K was used in the CMA code to determine the initial thickness of virgin carbon phenolic required for a given entry condition and the corresponding heating rates. An example result from a CMA computation at the stagnation point, showing the temperatures and the chemical reaction zones within the carbon phenolic, is presented in Fig. 13. Note that the peak ablation temperature reached 3500 K, but for only 1 s and to a depth of only 0.005 cm. At the temperatures shown in Fig. 13, spallation of the heat shield material should not be a major problem,[20] and the effect was ignored here. The result found from the stagnation-point CMA computations was that 0.0887 kg/MJ of virgin carbon phenolic material was needed to observe the 500 K temperature limit. To provide a safety margin, the above value was increased by 25%, yielding a final value of 0.111 kg/MJ. This heat shielding mass per unit heat load was applied to the heat loads shown in Fig. 12 to calculate the forebody heat shield mass fractions that are illustrated in Fig. 14. Note that the forebody heat shield mass fractions range from about 0.078 to 0.156, are nearly the same for both Uranus and Neptune, and depend only weakly on the ballistic coefficients. However, it should be emphasized, again, that the weak dependence on ballistic coefficient shown in Fig. 14 is the result, at least partially, of imposing the 400-g deceleration limit on all entry trajectories.

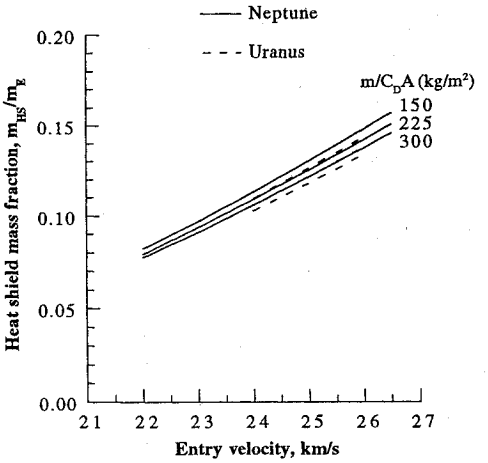

Fig. 14 Heat shield mass fraction as a function of entry velocity for Uranus and Neptune.

The mass losses from pyrolysis, other chemical reactions, and char removal were about 20% of the heat shield masses, or only about 2 to 4% of the bodies' initial masses, depending on the entry velocities.

It is instructive to compare the heat shield mass fractions shown in Fig. 14 with those of several other probes. The Pioneer-Venus large probe had a heat shield mass fraction of about 0.10 and discarded its heat shield at subsonic speeds.[21,22] The Pioneer-Venus small probes had heat shield mass fractions of about 0.13; however, the heat shields were not discarded during the long descent through the atmosphere. The forebody heat shield mass fraction of the Galileo probe is 0.43 and the heat shield is designed to be dropped at subsonic speeds.[23] Lastly, in a recent study[24] of the forebody heat shielding requirements for capsules that were intended to return cometary nucleus samples to Earth at a speed of 16.5 km/s, the heat shield mass fractions were found to be slightly over 0.2. The calculated heat shield mass fractions found for the Uranus and Neptune probes (0.08 to 0.16) are reasonable in view of past and future entry mission requirements.

Concluding Remarks

Studies of probes entering into the atmospheres of Uranus and Neptune have been made. It was shown that the steep entry angles that were needed to facilitate communication from the probes to the spacecraft buses could be met by using the Galileo Jupiter probe configuration and aeroshell structural design, which had a 400-g limit. However, the Uranus and Neptune capsules require much less heat shielding, since the probes enter the atmospheres of these outer planets at roughly half the velocity encountered by the Galileo probe at Jupiter. It was assumed that the probes used the same carbon phenolic heat shield material as the Galileo probe and the four successful Pioneer-Venus probes. The heating of the outer-planet probes was almost entirely from convection, with peak turbulent convective heating rates exceeding 6 kW/cm^2 at the highest entry speeds that were considered at both planets. The maximum heating rates were only about 25% of the peak value that is expected during the Jupiter entry of the Galileo probe. The outer-planet probe forebody heat shield mass fractions were found to vary from about 0.08 to 0.16 over the entry velocity range from 22 to 26.5 km/s, respectively. The heat shield mass fractions are in the same range as the 0.10 to 0.13 used on the Pioneer-Venus probes, but much less than the 0.43 required to protect the Galileo probe's forebody during its 48-km/s entry. If the Galileo probe's entry is successful, an outer-planet entry technology base, including heat shield design, should be well established and can be applied to refine the present results.

References

[1]Burns, J. A., "Neptune and Triton," *Icarus, International Journal of the Solar System*, Vol. 99, No. 2, 1992, p. 241.

[2]Swenson, B. L., and Wercinski, P. F., "Deep Atmospheric Probe Missions to Uranus and Neptune," AIAA Paper 90-2893, Aug. 1990.

[3]Swenson, B. L., "Neptune Probe Deployment and Design Issues," Science Applications International Corp., SAIC-91/1183, Los Altos, CA, Sept. 1991.

[4]Tauber, M. E., "Heat Protection for Atmospheric Entry into Saturn, Uranus and Neptune," *Advances in the Astronautical Sciences—The Outer Solar System*, edited by J. Vagners, Vol. 29, Part 2, American Astronautical Society, Tarzana, CA, 1971, pp. 215–228.

[5]Swenson, B. L., private communication, Science Applications International Corp., Los Altos, CA, Nov. 1992.

[6]Horton, T. E., and Menard, W. A., "A Program for Computing Shock-Tube Gasdynamic Properties," Technical Report 32-1350, Jet Propulsion Laboratory, Pasedena, CA, Jan. 1969.

[7]Liu, C. H., and Howe, J. T., "Outer Planet Entry—Radiating Shock Layer with Coupled Ablation for Carbon and Silica," AIAA Paper 76-472, July 1976.

[8]Moss, J. N., and Simmonds, A. L., "Galileo Probe Forebody Flowfield Predictions," AIAA Paper 82-0874, June 1982.

[9]Tauber, M. E., and Wakefield, R. M., "Heating Environment and Protection During Jupiter Entry," *Journal of Spacecraft and Rockets*, Vol. 8, No. 6, 1971, pp. 630–636.

[10]Tauber, M. E., "A Review of High-Speed Convective Heat Transfer Computation Methods," NASA TP-2914, July 1989.

[11]Gordon, S., and McBride, B. J., "Computer Program for Calculation of Complex Chemical Equilibrium Compositions, Rocket Performance, Incident and Reflected Shocks, and Chapman-Jouguet Detonations," NASA SP-273, Interim Revision, March 1976.

[12]Sutton, K., and Graves, R. A., Jr., "A General Stagnation-Point Convective-Heating Equation for Arbitrary Gas Mixtures," NASA TR R-376, Nov. 1971.

[13]Tauber, M. E., Yang, L., and Paterson, J.,"Flat Surface Heat-Transfer Correlations for Martian Entry," *Journal of Spacecraft and Rockets*, Vol. 30, No. 2, 1993, pp. 164–169.

[14]Marvin, J. G., and Pope, R. B., "Laminar Convective Heating and Ablation in the Mars Atmosphere," *AIAA Journal*, Vol. 5, No. 2, 1967, pp. 240–248.

[15]Green, M. J., and Davy, W. C., "Galileo Probe Forebody Thermal Protection," AIAA Paper 81-1073, June 1981.

[16]Bartlett, E. P., and Kendall, R. M., "An Analysis of the Coupled Chemically Reacting Boundary Layer and Charring Ablator," Part III, NASA CR-1062, June 1968.

[17]Anon., "Aerotherm Charring Material Thermal Response and Ablation Program (CMA87S)," Acurex Report UM-87-13/ATD, Mountain View, CA, Nov. 1987.

[18]Davy, W. C., Menees, G. P., Lundell, J. H., and Dickey, R. R., "Hydrogen-Helium Ablation of Carbonaceous Materials: Numerical Simulation and Experiment," AIAA Paper 78-866, May 1978.

[19]Williams, S., and Curry, D. M., "Thermal Protection Materials," NASA Reference Publication 1289, Dec. 1992.

[20]Lundell, J. H., and Dickey, R. R., "Ablation of Graphitic Materials in the Sublimation Regime," *AIAA Journal*, Vol. 13, No. 8, 1975, pp. 1079–1085.

[21]Wakefield, R. M., and Pitts, W. C., "Analysis of the Heat-Shield Experiment on the Pioneer-Venus Entry Probes," AIAA Paper 80-1494, July 1980.

[22]Pitts, W. C., and Wakefield, R. M.,"Performance of Entry Heat Shields on Pioneer-Venus Probes," *Journal of Geophysical Research*, Vol. 85, No. A13, Dec. 30, 1980, pp. 8333–8337.

[23]Givens, J. J., Nolte, L. J., and Pochettino, L. R., "Galileo Atmospheric Entry Probe System: Design, Development and Test," AIAA Paper 83-0098, Jan. 1983.

[24]Henline, W., and Tauber, M. E., "Trajectory-Based Heating Analysis of the ESA/Rosetta Earth-Return Vehicle," AIAA Paper 93-0269, Jan. 1993.